Structural connectivity in schizophrenia and its impact on the dynamics of spontaneous functional networks

Joana Cabral,[1,2] Henrique M. Fernandes,[2,3] Tim J. Van Hartevelt,[2,3] Anthony C. James,[2,4] Morten L. Kringelbach,[2,3] and Gustavo Deco[1,5]
[1]*Theoretical and Computational Neuroscience Group, Center of Brain and Cognition, Universitat Pompeu Fabra, Barcelona 08018, Spain*
[2]*Department of Psychiatry, University of Oxford, Oxford OX3 7JX, United Kingdom*
[3]*Center of Functionally Integrative Neuroscience (CFIN), Aarhus University, Aarhus, Denmark*
[4]*Highfield Unit, Warneford Hospital, Oxford OX3 7JX, United Kingdom*
[5]*Institució Catalana de Recerca i Estudis Avançats (ICREA), Barcelona 08010, Spain*

(Received 21 March 2013; accepted 5 December 2013; published online 23 December 2013)

The neuropathology of schizophrenia remains unclear. Some insight has come from modern neuroimaging techniques, which offer an unparalleled opportunity to explore *in vivo* the structure and function of the brain. Using functional magnetic resonance imaging, it has been found that the large-scale resting-state functional connectivity (rsFC) in schizophrenia — measured as the temporal correlations of the blood-oxygen-level-dependent (BOLD) signal — exhibit altered network topology, with lower small-world index. The origin of these rsFC alterations and link with the underlying structural connectivity remain unclear. In this work, we used a computational model of spontaneous large-scale brain activity to explore the role of the structural connectivity in the large-scale dynamics of the brain in health and schizophrenia. The structural connectomes from 15 adolescent patients with early-onset schizophrenia and 15 age- and gender-matched controls were built from diffusion tensor imaging data to detect the white matter tracts between 90 brain areas. Brain areas, simulated using a reduced dynamic mean-field model, receive excitatory input from other areas in proportion to the number of fibre tracts between them. The simulated mean field activity was transformed into BOLD signal, and the properties of the simulated functional networks were analyzed. Our results suggest that the functional alterations observed in schizophrenia are not directly linked to alterations in the structural topology. Instead, subtly randomized and less small-world functional networks appear when the brain operates with lower global coupling, which shifts the dynamics from the optimal healthy regime.
[http://dx.doi.org/10.1063/1.4851117]

Brain activity during rest displays the spontaneous formation and dissolution of large-scale functional networks, most of which are typically activated during specific tasks. This phenomenon is believed to reflect noise excursions from the stable equilibrium state into "ghost" attractor states present in the brain's dynamical repertoire. While these patterns are robust across healthy people, they appear disrupted in people with schizophrenia. Here, we investigate the causes of this disruption. Our results indicate that the functional alterations observed in schizophrenia may be due to a decrease in the global coupling weight between brain areas, which shifts the dynamical regime further below the bifurcation, leading to fewer excursions and therefore more random and less small-world functional networks.

I. INTRODUCTION

The brain is one of the most complex networks in nature. Modern neuroimaging techniques have helped to detect *in vivo* the map of structural and functional connections in the brain. In particular, the structural connections between brain regions, which are mediated by white matter fibres, can be detected using diffusion magnetic resonance imaging (diffusion-MRI).[1,2] On the other hand, functional connections are typically inferred from temporal correlations between neural activity measures, such as the blood-oxygen-level-dependent (BOLD) signal obtained from functional-MRI (fMRI).[3,4] Although the structural connections remain mostly unchanged over short periods in time, the functional connections can be increased or decreased depending on the cognitive task the subject is performing. Interestingly, during rest, i.e., in the absence of any explicit task, the same functional networks that are typically observed during task appear temporarily activated on a very slow time scale (i.e., <0.1 Hz).[5] This spontaneous activity is thought to reveal intrinsic properties of the brain's network dynamics and has attracted a growing body of theoretical and computational neuroscience research.[6–9]

Recently, Deco and Jirsa proposed that the emergence and dissolution of functional networks during rest is the result of noisy excursions into latent "ghost" attractor states.[10] In this theoretical framework, the resting brain operates at the brink of a bifurcation that separates the stable low-activity equilibrium state from the multi-stable state region where many attractors coexist. This multi-stable attractor landscape

defines a functionally meaningful dynamic repertoire of the brain, which is inherently defined by the neuro-anatomical network structure.

The optimal balance of the brain at rest has proved essential for an optimal cognitive function. Indeed, over the last decade, a large number of studies have reported altered resting brain activity in a wide range of mental illnesses, including schizophrenia (see below), Alzheimer's disease,[11–14] dementia,[15,16] autism,[17,18] mild cognitive impairment,[19] multiple sclerosis,[20] and major depression.[21,22] These results not only illustrate the importance of balancing resting-state dynamics but also provide insights to understand the intrinsic mechanisms leading to and potentially treating the diseased brain.[23]

Regarding schizophrenia, several studies have reported a widespread decrease in the functional connectivity (FC) of patients during rest, supporting the hypothesis that schizophrenia may arise from the disrupted functional integration of segregated brain areas.[24–27] Further analysis of resting-state functional networks in schizophrenia using graph theory indicate a subtle randomization of functional networks, with decreased small-world properties, lower clustering coefficients, and fewer high-degree hubs.[25,28,29] In addition, some topological measures such as the small-world index were found to correlate with cognitive performance,[25] indicating that resting-state correlations may be closely related to the binding mechanisms that support the integration of information in the brain. In this work, we used data from a group of adolescent patients with early-onset schizophrenia, which possibly represent a more severe form of the disease.[30,31]

In this work, we aim to investigate, from a dynamical system's perspective, what occurs in schizophrenia to cause the disruption of resting-state functional connectivity. Previous studies have revealed that resting-state functional networks reflect, to some extent, the underlying structural connectivity. However, the relationship between the functional alterations observed in schizophrenia and the underlying structural connectivity is not straightforward, and computational models, like the one presented here, are valuable tools to investigate this non-trivial relationship.[32]

We start by comparing the structural connectomes from patients and healthy controls in terms of global topological properties, such as connection density, number of fibre tracts per connection, clustering coefficient, path length, small-world index and hierarchy, among others. Subsequently, to investigate the dynamical impact of the structural changes occurring in schizophrenia, we used a reduced dynamic mean-field model of spontaneous activity.[33] The spontaneous dynamics obtained with the different structural connectomes, i.e., from patients and healthy controls, was analyzed and the BOLD functional connectivity was predicted as a function of the global coupling weight. Our results suggest that the disruption of functional networks in schizophrenia may not be directly induced by the alterations observed in the structural connectomes from patients. Instead, it might be related to a decrease in the global coupling weight, which shifts the dynamics to a regime with fewer excursions to latent ghosts attractors leading to more random functional connectivity.

II. METHODS AND MEASURES

A. Patients

The study was undertaken in accordance with the guidance of the Oxford and Berkshire Psychiatric Research Ethics Committees and written consent was obtained from all participants (and their parents if under the age of 16 years).

We acquired structural data from fifteen adolescent patients (8 males and 7 females, age: 14–17 years, mean 15.97) who were diagnosed as having DSM-IV[34] schizophrenia, using the Kiddie Schedule for Affective Disorders and Schizophrenia.[35] In addition, the symptom severity was measured using the Positive and Negative Syndrome Scale (PANSS), which consists in an interview to evaluate the degree of positive (referring mainly to hallucinations, delusions, excitability, suspiciousness, etc.) and negative symptoms (representing a diminution or loss of functions such as anergia, poverty of thinking, etc.) in schizophrenia.[36] Age at onset of symptoms ranged from 13 to 16 years. All schizophrenic patients were receiving atypical antipsychotics.

Furthermore, we acquired control data from fifteen healthy control participants who were matched for age and sex to the adolescent-onset patient group (6 males and 9 females, age: 14–17 years, mean 16.03). The adolescent control participants were recruited from the community through their general practitioners and were screened for any history of emotional, behavioural, or medical problems. All participants attended normal schools. Exclusion criteria included moderate mental impairment ($IQ < 60$), a history of substance abuse or pervasive developmental disorder, significant head injury, neurological disorder or major medical disorder (for more details see Douaud *et al.*[37]).

B. Structural connectivity data

Anatomic brain networks were constructed using diffusion tensor imaging (DTI). All participants underwent the same imaging protocol with a whole-brain T1-weighted and diffusion-weighted scanning using a 1.5 T Sonata MR imager (Siemens, Erlangen, Germany) with a standard quadrature head coil and maximum 40 mT m^{-1} gradient capability. The 3D T1-weighted FLASH sequence was performed with the following parameters: coronal orientation, matrix 256×256, 208 slices, 1×1 mm^2 in-plane resolution, slice thickness 1 mm, TE/TR = 5.6/12 ms, flip angle $\alpha = 19°$. Diffusion-weighted images were obtained using echo-planar imaging (SE-EPI, TE/TR = 89/8500 ms, 60 axial slices, bandwidth = 1860 Hz/vx, voxel size $2.5 \times 2.5 \times 2.5$ mm^3) with 60 isotropically distributed orientations for the diffusion-sensitising gradients at a b-value of 1000 s mm^{-2} and 5 $b = 0$ images.[38] To increase signal-to-noise ratio, scanning was repeated three times and all scans were merged.

The parcellation of the entire brain in native DTI space into 90 cortical and subcortical regions (45 for each hemisphere (Ref. 39)), was accomplished by using the Automated Anatomic Labelling (AAL) template, where each region represents a node of the brain network.[40] We used Flirt (FSL, Oxford)[41] to co-register the b0 image in diffusion MRI space

to the T1 template of ICBM152 in MNI (Montreal Neurological Institute) space.[42] The resulting transformation was then inversed and applied to warp the AAL template from the MNI space to the native DTI space. Interpolation with the nearest-neighbour method was used to ensure that discrete labelling values were preserved.

We used the Fdt toolbox in FMRIB Software Library (FSL) where FMRIB stands for Functional Magnetic Resonance Imaging of the Brain (www.fmrib.ox.ac. uk/fsl/, Oxford) to process the diffusion MRI data. The initial preprocessing involved the coregistration of the diffusion-weighted images to a reference volume using an affine transformation for the correction of head motion and eddy current gradient induced image distortion. We further modeled crossing fibers within each voxel, and estimated the local probability distribution of fibre direction at each voxel of the brain.[43,44]

We estimated the connectivity probability from each seed region to the 89 other brain regions (using in-house Perl scripts) by applying probabilistic tractography, using a sampling of 5000 streamline fibres per voxel. The connectivity probability from a seed voxel i to voxel j was defined as the proportion of fibres passing through voxel i that reach voxel j.[44] This was then extended from the voxel level to the region level, and the connectivity probability P_{ij} from region i to region j was then calculated as the number of sampled fibres in region i that connect the two regions divided by 5000*n, where n is the number of voxels in region i.

Despite the dependence of tractography on the seeding location, the probability from i to j and j to i is highly correlated across the brain for all participants (the least Pearson $r = 0.70$, $p < 10 - 50$). Therefore, we defined the undirectional connectivity probability P_{ij} between regions i and j by averaging the two probabilities, and considered this as a measure of the structural connectivity between two areas, with $C_{ij} = C_{ji}$.

We used in-house Perl scripts to implement the calculation of regional connectivity probability. For each subject, a 90×90 weighted network was constructed, representing the anatomical network of the brain. In addition, averaged connectivity matrices, $C_{Patients}$ and $C_{Controls}$, were constructed for each group of participants.

C. The dynamic mean field model

To investigate the dynamics emerging from the structural connectomes, we used a dynamic mean-field model for each of the 90 brain areas, and coupled them together according to the anatomical structural connectome. The classical mean field model is used to calculate the steady states of a network of densely interconnected spiking neurons.[45] However, since we are interested on the temporal dynamics of this mean field (to investigate temporal correlations between brain areas), we use a dynamic mean-field model which includes an approximation of the temporal dynamics of the spiking network.[33] The dynamic mean-field approximation defines the collective dynamics of excitatory and inhibitory spiking neurons interconnected by AMPA, GABA, and NMDA receptors and their respective equations, reducing the spiking network model to a single dimensional equation. In this approximation, the behaviour of interacting brain areas can be described by the following set of coupled differential equations,

$$\frac{dS_n(t)}{dt} = -\frac{S_n}{\tau_S} + (1 - S_n)\gamma H(x_n) + \sigma \upsilon_n(t), \tag{1}$$

$$H(x_n) = \frac{ax_n - b}{1 - \exp(-d(ax_n - b))}, \tag{2}$$

$$x_n = wJ_N S_n + WJ_N \sum_p C_{np} S_p + I_0, \tag{3}$$

S_n denotes the average synaptic gating variable at the local cortical area n ($n = 1,\ldots,N$, where N is the total number of nodes). x_n is the total input current in area n and $H(x_n)$ is a transduction function that transforms the input current into the population firing rate. $w = 0.9$ is the weight of local excitatory recurrence and C_{np} is coupling weight between the areas n and p, defined as the number of fibres detected from DTI, and varies from subject to subject. W is the global coupling weight that scales C uniformly and is the only parameter that we vary in this work. Parameter values for the input–output function (2) are $a = 270$ VnC, $b = 108$ Hz, and $d = 0.154$ s. $\tau_s = 100$ ms is the decay time constant of S and H (in Hz) is divided by 1000 for unit consistency. $\gamma = 0.641$ is a constant related to the magnesium concentration controlling the NMDA currents (see Theodoni *et al.* (Ref. 46)). The synaptic couplings are $J_N = 0.2609$ nA and the overall effective external input is $I_0 = 0.3$ nA. In Eq. (1), υ_i is uncorrelated standard Gaussian noise and the noise amplitude at each node is $\sigma = 0.001$ nA. Model parameters were defined in Deco *et al.*[33] to be consistent with a detailed spiking model validated to reflect neurophysiology.[10]

Simulations were run for increasing values of global coupling weight W, using the structural connectivity matrices from the 15 patients with schizophrenia and the 15 healthy controls. The critical coupling weight, $W_{crit,}$ was identified by detecting the coupling weight above which the equilibrium state becomes unstable, i.e., when the mean synaptic activity, $\langle S \rangle$, crosses a threshold of 0.3 after a transient period of 10 s.

D. Simulated functional connectivity

To explore the relationship between structural and functional connectivity in schizophrenia, we used the Balloon-Windkessel model[47] to transform the simulated mean field activity into BOLD signal.[9,10,33] This model describes the transduction of neuronal activity (given by the level of synaptic activity, S_n) into perfusion changes and subsequently into BOLD signal. The simulated BOLD signal was down-sampled at 2 s to have the same temporal resolution as in the empirically measured BOLD signal (see Sec. II E). The simulated FC is given by the correlation matrix of the simulated BOLD signals in each brain area. For each group-averaged structural connectomes, $C_{Patients}$ and $C_{controls}$, the resulting functional connectivity (FC) matrices were calculated for a range of global coupling weights, W (see Figure 1 for an illustration).

E. Empirical functional connectivity

The different FCs simulated with the model (i.e., obtained with $C_{Patients}$ and $C_{Controls}$ and for increasing global

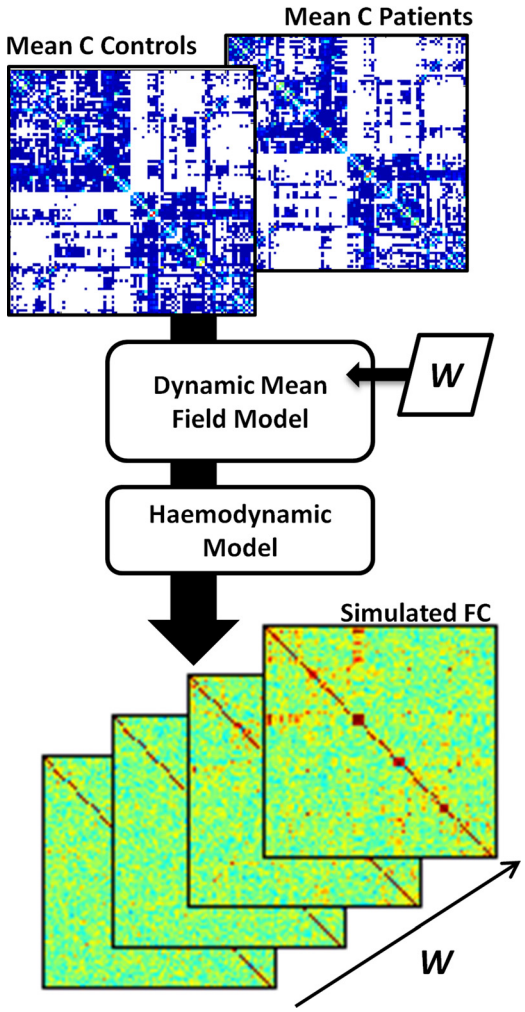

FIG. 1. Diagram illustrating the steps to obtain the simulated functional connectivity matrices. Using the average structural connectomes (C) from each group of subjects (i.e., 15 healthy controls or 15 patients with schizophrenia), we model the behaviour of coupled brain areas using a dynamic mean-field model and vary the global coupling weight W. For each W, the simulated mean field activity at each node is transformed into BOLD signal using the Balloon-Windkessel haemodynamic model and the correlation matrices are computed to obtain the simulated FCs.

coupling weights W) were compared with the functional connectivity measured between the same 90 brain areas averaged across 18 healthy subjects provided to us by He and colleagues.[48] This empirical FC matrix represents the average FC obtained from 18 right-handed healthy young volunteers at rest (9 females, age range of 21–25 years). The subjects were scanned using a 3T GE MR scanner (EXCITE, Milwaukee, USA). The images were obtained using an EPI sequence with the following parameters: 30 axial slices, slice thickness = 4.5 mm with no gap, matrix = 64×64, TR = 2000 ms, TE = 30 ms, flip angle = 90°, field of view = 220×220 mm^2. Subjects were instructed to lay completely still, keep their eyes closed and relax their minds as much as possible. See Wang *et al.*[49] for a full description of the pre-processing of the resting-state fMRI data.

To compare the simulated FCs with the real one, we computed the Pearson correlation between values in the upper-triangular part of the FC matrices (excluding the diagonal), as in Deco *et al.*[33]

F. Evaluating network properties

The structural brain networks derived from DTI can be represented as 90×90 connectivity matrices, C, where each entry in the matrix C_{np} indicates the number of fibre tracts detected between the areas n and $p, \forall n, p \in N$). To compare the structural networks from patients and controls at a global level, we defined a number of measures, some of which from graph theory, and tested for their significance using the two-sample Kolmogorov-Smirnov test.[50]

First, for each subject, we calculate the total number of fibre tracts detected between brain areas. Second, considering that two brain areas are connected if at least one fibre tract is detected between them, we estimate the connection density, or cost, of the networks. The cost is given as the percentage of existing connections, divided by the total number of possible connections ($(N^2 - N)/2$). Subsequently, we estimate the average number of fibre tracts detected per connection and its variance.

To gain information about the topological organization of brain networks we estimated some measures from graph theory with the help of the Brain Connectivity Toolbox,[51] namely:

Degree. The degree of a node d(n) is taken as the number of nodes to which node n is connected.

Characteristic path length. The shortest path length between areas n and p is the minimum number of connections that are needed to connect regions n and p. The characteristic path length is given as the mean shortest path length over all pairs of nodes in the network.

Clustering coefficient. The clustering coefficient of a node n indicates the fraction of a node's neighbours (i.e., connected to node n) that are also neighbours of each other. The network clustering coefficient is taken as the average clustering coefficient of all nodes in the network.

Small-worldness. One of the most striking and widely studied properties of brain networks is their small-world organization.[52–55] A network C is considered to be small-world ($\sigma > 1$), if the characteristic shortest path length is small and the clustering coefficient is high, when compared to an equivalent random graph R.[56] The small-world architecture is particularly rich in complex brain networks because it supports both segregated specialization and distributed integration, maximizing the information transfer at a relatively low wiring cost. The importance of a small-world topology for an optimal cognitive performance is corroborated by reports of disrupted small-world properties of functional networks in diseases such as schizophrenia,[25,28,29] Alzheimer's disease[14] and attention-deficit/hyperactivity disorder.[57] As such, here we investigate for which model parameters the simulated functional networks have typical small-world properties from health and schizophrenia.

The network measures defined in this section were calculated for all subject's structural connectomes. We used the two-sample Kolmogorov-Smirnov test[50] and the Mann-Whitney U-test[58] to evaluate if the differences between patients and controls are statistically different. Both tests evaluate the likelihood that the values from the 2 groups belong to the same continuous distribution (if $p > 0.05$). However, while

the Kolmogorov-Smirnov is more sensitive to the difference between means, the Mann-Whitney is more sensitive to the difference between medians, and as such is more robust against outliers.

To evaluate the topological organization of the functional networks obtained with the model, we estimated the small-world index as a function of the global coupling weight W. Since the functional connectivity represents the correlation between BOLD signals, it is necessary to define a correlation threshold above which a functional connection is considered a link. This threshold needs to be defined as a function of the connection density,[25,29] since networks need to have the same number of nodes and the same number of links for a reliable comparison. As such, the properties of the functional networks were estimated for a range of connection densities, and subsequently averaged across this range. Here, we defined the range of thresholds in order to match the small-world index of the best simulated healthy FC before the bifurcation (i.e., where the fit with empirical healthy FC was optimal, $W = 1.3$) with the small-world index reported in Lynall *et al.* for healthy controls ($\sigma = 1.614$). Since in Lynall *et al.* only 72 of the 90 AAL brain areas were considered, we selected only the same 72 brain areas for this comparison.[39] This resulted in a threshold range between 23% and 33%. All other analyses were performed in networks containing all the 90 brain areas.

III. RESULTS

First, the structural networks from the brains of patients and controls were compared taking into account the total number of fibres, the number of fibres per connection and the connection density but no statistically significant differences were found between groups in these general measures (Figure 2 and Table I). In addition, structural networks were compared in terms of their topological organization using some typical measures from graph theory, such as the characteristic path-length, the clustering coefficient, the mean degree, and the small-world index. From the graph-theoretical perspective, some measures showed significant differences between patients and controls, in particular when using the Mann-Whitney U-test to test for statistical significance ($p < 0.05$).

Second, we investigated if the structural connectivity from patients with schizophrenia induced alterations at the dynamical level using a whole-brain model of spontaneous activity (see Sec. II C for details). For such, we simulated the dynamics obtained with the model using the structural connectomes from the 15 patients and the 15 controls. The main parameter varied in the model was the global coupling weight W. In Deco *et al.*[33] it was found that the model optimally reproduced spontaneous healthy FC when W was set below a critical value W_{crit}. As such, we investigated if the structural connectivity from patients with schizophrenia induces a shift in W_{crit}. As shown in Figure 3(a), the mean W_{crit} appeared lower in patients ($W_{crit} = 1.36 \pm 0.12$ for controls and $W_{crit} = 1.29 \pm 0.11$ for Patients; mean $\pm$ standard deviation). However, the difference was not significant as it did not reject the null hypothesis with >95% confidence (p-value $= 0.052$ using the 2-sample Kolmogorov-Smirnov test). Using the average structural connectomes from patients and controls instead of the individual ones (Figure 3(b)), we also found the difference to be negligible: W_{crit} $C_{Controls} = 1.404$ and W_{crit} $C_{Patients} = 1.408$. For a range of coupling weights falling before this critical value ($1.25 < W < 1.35$) the simulated FCs optimally approximate the empirical one (Pearson correlation $\rho > 0.3$), as observed in a previous implementation of the model.[33] Notably, an optimal fit with empirical healthy FC can be obtained not only with the connectomes from controls but also with the connectomes from patients, without any significant difference between groups (Figure 3(c)).

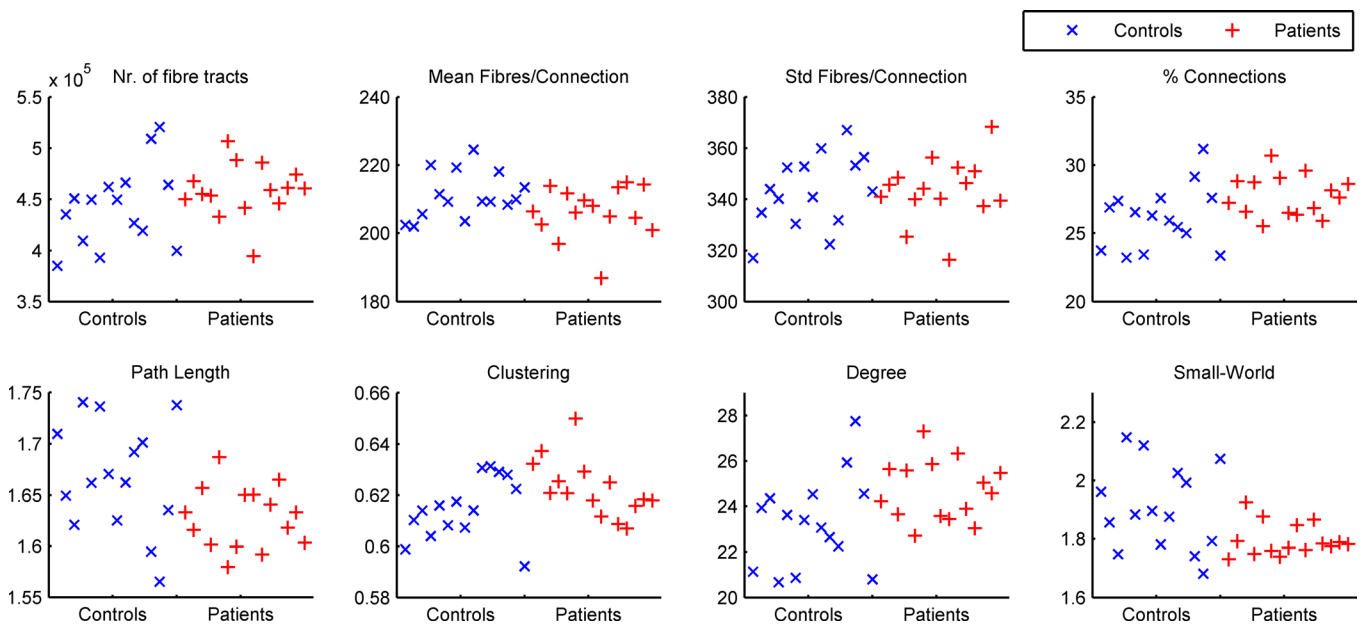

FIG. 2. Properties of the structural networks from patients and controls. In each plot, the structural connectivity properties of 15 healthy controls (×) and 15 patients with schizophrenia (+) are reported (see Table I). Std, standard deviation.

TABLE I. Group differences between structural networks from patients and controls. Std., standard deviation. The significance was estimated using the two-sample Kolmogorov-Smirnov test. Measures that rejected the null hypothesis with >95% confidence are marked with (*).

	Controls		Patients		Kolmogorov-Smirnov test	Mann-Whitney U-test
	Mean	Std	Mean	Std	*p*-value	*p*-value
Total fibres	4.425×10^5	3.932×10^4	4.583×10^5	2.619×10^4	0.307	0.171
Fibres/connection (mean)	211.096	6.803	206.335	7.572	0.308	0.199
Fibres/connection (std)	343.051	14.144	343.433	12.259	0.589	0.934
Connection density	26.180	2.265	27.742	1.494	0.136	0.421
Clustering coefficient	0.615	0.012	0.622	0.011	0.136	0.106
Path length	1.667	0.053	1.628	0.030	0.052	0.031*
Degree (mean)	23.301	2.016	24.690	1.330	0.136	0.042*
Small-world index	1.905	0.145	1.796	0.056	0.052	0.034*

Although no differences were detected in the critical coupling weight between patients and controls, subtle structural differences occurring in the disease may have an impact in the topological organization of functional connectivity. Following reports of less small-world resting-state functional networks in schizophrenia,[25,28,29] we investigated the small-world index of the FCs simulated with the connectomes from patients and controls. As shown in Figure 4, for the same coupling weight, the small-world index did not appear significantly reduced in patients. What is more, in the region of optimal fit with empirical healthy FC, the FCs simulated with the patients' structural connectome sometimes even exhibited higher small-worldness than the FCs obtained with the average connectome from controls. This suggests that the topological alterations observed in functional networks in schizophrenia (such as a reduced small-world index) may not be directly linked to changes in the structural connectivity but to other factors influencing the brain's spontaneous dynamics in the disease. As a matter of fact, it can be seen in Figure 4 that the small-world index is sensitive to the coupling weight, increasing continuously until the critical coupling weight and then returning to low values after the bifurcation. In the range of coupling weights where the simulated FCs optimally reproduce the empirical healthy FC ($W \sim 1.30 \pm 0.5$), the small-world properties are in the range of the ones reported for healthy subjects in Lynall *et al.*, $\sigma_{\text{Controls}} = 1.614 \pm 0.0745$. Lower small-world indexes like the ones reported in schizophrenia ($\sigma_{\text{Patients}} = 1.5300 \pm 0.1184$)[25] could be obtained in the model by setting the global coupling weight in the range between $1 < W < 1.30$. When the global coupling weight is decreased in the model, the dynamical regime of the system is moved in the direction of the stable low-activity equilibrium state leading to more random and consequently less-small world functional networks. These results suggest that the behavioural symptoms observed in schizophrenia may be originated by a decrease in the coupling weight which

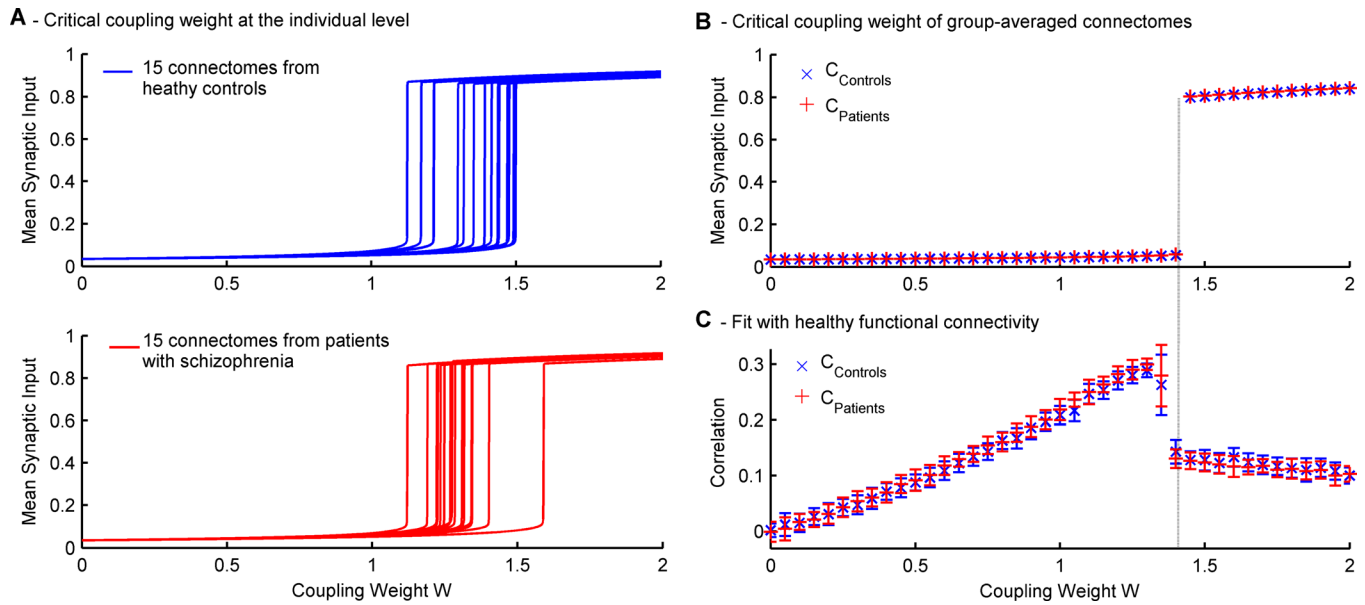

FIG. 3. Dynamical behaviour of the model obtained with the connectomes from patients (red) and controls (blue). (a) The critical coupling weight (W_{crit}) can be determined from simulations by detecting the coupling weight above which the average synaptic input $<S_n>$ increases from the low firing equilibrium state to a high firing state. As such, vertical lines indicate the W_{crit} of the corresponding connectomes. (b) Same as (a) but estimated for the average connectome from patients, $C_{Patients}$, and the average connectome from controls, $C_{Controls}$. (c) Correlation between the simulated functional connectivity matrices (FC)—obtained with $C_{Patients}$ (red) and $C_{Controls}$ (blue)—and the empirical healthy FC, as a function of the global coupling weight (W). Error bars indicate the mean and standard deviation across 20 simulations (None of these values was significantly different between groups: $p > 0.05$, for all W). The vertical dashed line indicates the critical coupling weight W_{crit} defined in (b).

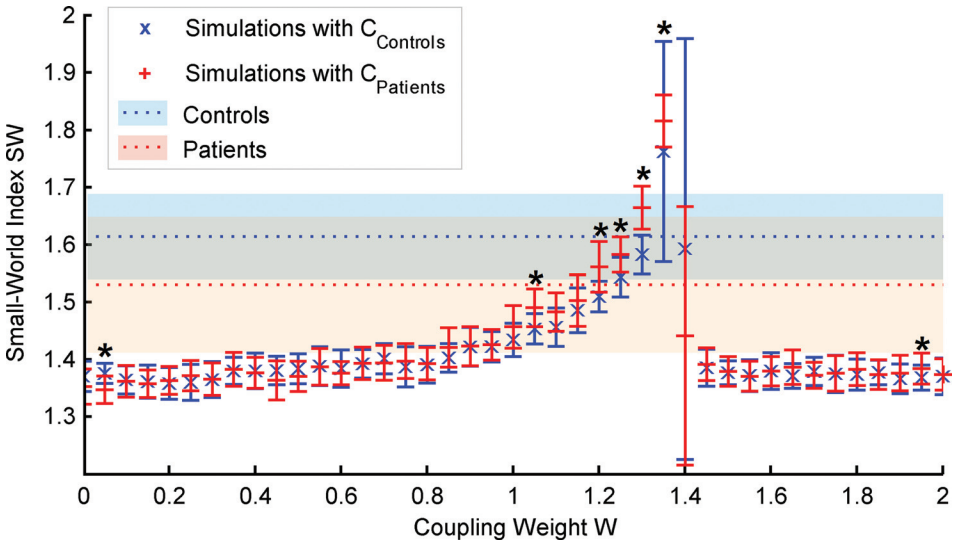

FIG. 4. Small-world index of simulated FC as a function of the global coupling weight W and comparison with values reported in the literature. Simulated data obtained with the structural connectomes from controls (blue) and patients (red). Error bars indicate the mean and standard deviation across 20 simulations (* indicate values significantly different between groups: $p < 0.05$). The dotted lines and shades represent the empirical values (mean and standard deviation) reported for functional networks in health and schizophrenia.[25]

leads to a shift from the healthy spontaneous regime—at the border of the bifurcation—towards the stable low-activity equilibrium state.

IV. DISCUSSION

Several experimental and theoretical studies indicate that resting-state functional connectivity is strongly shaped by the underlying structural connectivity.[7,33,59] However, the fact that functional networks appear subtly randomized in schizophrenia does not necessarily mean that the long-range white matter fibres connecting brain areas are more randomly distributed.[25,27–29] In the present work, we use for the first time structural connectomes from adolescents with early-onset schizophrenia and controls together with a computational model of whole-brain spontaneous activity in order to investigate the causes of disrupted resting-state functional connectivity in the disease.

Analysing the connectomes from patients and controls at the structural level, significant differences could only be found at the level of their topological organization, and only when using the Mann-Whitney U-test, which is more robust against outliers. In particular, the structural connectomes from patients had lower path length, higher mean degree and lower small-world index. These results point to the direction that, even if the connectomes from patients have a similar number of links as controls, these links are organized differently and this (dis)organization could potentially affect normal brain function originating the behavioural symptoms observed in schizophrenia.

To investigate the impact of these structural alterations in the spontaneous functional connectivity, the spontaneous activity was simulated for the different structural connectomes using the reduced mean field model. Although the critical coupling weight appeared to be sensitive to subtle structural differences existing between subjects, it did not differ significantly between groups. This suggests that, at least from the perspective of the current model, the structural connectivity of patients with schizophrenia does not affect the dynamical regime of the system. However, this paper shows only one of the possible mechanisms by which the altered functional connectivity in schizophrenic patients could be explained, and an influence of structural connectivity cannot be completely ruled out.

Analysing the simulation results in terms of spontaneous BOLD functional connectivity, an optimal fit with empirical healthy functional connectivity could be obtained with both the connectomes from controls and patients, as long as the coupling weight was set within an optimal range before the critical value. Indeed, as shown in Deco *et al.*,[33] this is where the functional connectivity maximally expresses the underlying structural connectivity. Even so, the maximum correlation obtained between real and simulated functional connectivity was only slightly above 0.3 for both groups. As such, the functional networks resulting from the different structures could still differ in topology even if they showed a similar correlation coefficient with real healthy functional connectivity.

As the resting-state functional networks from patients with schizophrenia have been found to be less small-world than healthy controls *and* the structural networks from patients showed a trend to be less small-world, we expected the simulated functional networks to have a lower small-word index in the patients' group. However, we found that the simulated functional networks obtained with the patients' structural connectome sometimes even displayed a higher small-world index, making proof of the complex relationship between structural and functional connectivity. From the perspective of the current model, we found that the best way to obtain functional networks with small-world indexes matching the ones reported experimentally for patients[25] would be by adjusting the global coupling weight of the system. In other words, the small-world indexes reported for healthy people could be obtained in the range of coupling weights where a best fit with empirical FC was obtained, whereas the small-world indexes reported in schizophrenia could be obtained in the model by decreasing the global coupling weight.

From a physiological perspective, the global coupling weight in the model scales the strength of excitatory synaptic

input between brain areas. A decrease in this coupling weight could be, in general terms, related to any disruption of synaptic and/or axonal mechanisms. For example, there is convincing evidence that NMDA receptor hypofunction may contribute to the symptomatic features of schizophrenia,[60] which supports the findings in this study. In addition, it could also be related to reports of deficient synaptic plasticity[61] or malfunction in the dopaminergic,[62,63] glutamatergic,[64] or cholinergic[65,66] neurotransmission in schizophrenia. Importantly, the current model provides a global picture for the pathophysiology of schizophrenia, where the communication between brain areas is reduced, irrespective of the physiological mechanism causing it.

Note that the hypothesis of a decreased coupling strength between brain areas in schizophrenia has been already proposed in previous works.[32,67] In more detail, using two different models at the node level, it was found that the properties of resting-state functional networks in schizophrenia could be obtained by decreasing the global coupling strength. However, these studies used only the structural connectomes from healthy subjects, and therefore it was not possible to test if the same results could be obtained with connectomes from patients with schizophrenia. Here, our results indicate that the structural differences found between healthy controls and patients did not affect the spontaneous functional networks, corroborating previous theoretical predictions and extending them to early-onset schizophrenia which is clinically more severe than the adult-onset form of the disease.

In Deco and Jirsa,[10] it is proposed that the healthy resting brain operates at the brink of a bifurcation that separates the low-activity equilibrium state from the multistable state region where many attractors—corresponding to high activity in different brain areas—coexist. Under these conditions, the activation of resting-state networks occurs due to structured noise fluctuations around the low-activity state induced by the presence of latent "ghost" attractors at the edge of the bifurcation. In this theoretical scenario and in the light of the current results, we propose that the brains in schizophrenia are operating further below the bifurcation than healthy subjects and therefore fewer excursions to the "ghost" attractor states occur. Beyond the resting-state, one can speculate that this condition can explain the behavioural symptoms of schizophrenia, whose most characteristic sign is the disintegration of psychological functions resulting in a loss of unity of mind and consciousness.[68,69]

Furthermore, our results indicate that the spontaneous activity of people with schizophrenia could be balanced back to normal values if the global coupling weight between brain areas could be increased in some way, i.e., with the help of medication or using deep brain stimulation. Actually, we find that the FC matrices simulated with the model using the patient's structural connectomes can predict with good agreement the functional connectivity from healthy subjects (and with small-world properties that match the ones from controls) if the global coupling weight is tuned at an optimal value.

Despite providing a meaningful theoretical scenario, this work has several limitations. While the patient and control groups were matched for age and sex for the measures of structural connectivity, we were unable to obtain functional data from these groups. Instead, we had to use functional connectivity data from a slightly older control group. In addition, the topological properties of simulated functional networks were compared with the ones reported empirically from 15 healthy adult volunteers and 12 patients with schizophrenia.[25] In further studies, the employment of empirical functional data from the same patients and controls would be needed to validate the results reported herein. Although our model results do not indicate any direct influence of the structural connectivity in the topology of functional networks, it is important to note that our analysis was performed at a very low resolution (i.e., only 90 brain areas) and our model is (intentionally) very reduced. As such, the influence of structural connectivity on the functional topology cannot be ruled out.

ACKNOWLEDGMENTS

The research reported herein was supported by the ERC Advanced Grant DYSTRUCTURE (No. 295129), by the FET Flagship Human Brain Project, by the Spanish Research Project SAF2010-16085, by the CONSOLIDER-INGENIO 2010 Programme CSD2007-00012, by the Brain Network Recovery Group through the James S. McDonnell Foundation, by the FP7-ICT BrainScales, and by the TrygFonden Charitable Foundation. Funding for the scanning was supported by the MRC (G0500092).

[1]Y. Iturria-Medina, E. J. Canales-Rodriguez, L. Melie-Garcia, P. A. Valdes-Hernandez *et al.*, Neuroimage **36**, 645 (2007).
[2]P. Hagmann, M. Kurant, X. Gigandet, P. Thiran *et al.*, PLoS ONE **2**, e597 (2007)
[3]B. B. Biswal, M. Mennes, X. N. Zuo, S. Gohel *et al.*, Proc. Natl. Acad. Sci. U.S.A. **107**, 4734 (2010).
[4]B. Biswal, F. Z. Yetkin, V. M. Haughton, and J. S. Hyde, Magn. Reson. Med. **34**, 537 (1995).
[5]J. S. Damoiseaux, S. A. Rombouts, F. Barkhof, P. Scheltens *et al.*, Proc. Natl. Acad. Sci. U.S.A. **103**, 13848 (2006).
[6]A. Ghosh, Y. Rho, A. R. McIntosh, R. Kötter *et al.*, PLoS Comput. Biol. **4**, e1000196 (2008).
[7]C. J. Honey, O. Sporns, L. Cammoun, X. Gigandet *et al.*, Proc. Natl. Acad. Sci. U.S.A. **106**, 2035 (2009).
[8]G. Deco, V. Jirsa, A. R. McIntosh, O. Sporns *et al.*, Proc. Natl. Acad. Sci. U.S.A. **106**, 10302 (2009).
[9]J. Cabral, E. Hugues, O. Sporns, and G. Deco, Neuroimage **57**, 130 (2011).
[10]G. Deco and V. K. Jirsa, J. Neurosci. **32**, 3366 (2012).
[11]M. D. Greicius, G. Srivastava, A. L. Reiss, and V. Menon, Proc. Natl. Acad. Sci. U.S.A. **101**, 4637 (2004).
[12]J. S. Damoiseaux, K. E. Prater, B. L. Miller, and M. D. Greicius, Neurobiol. Aging **33**, 828.e19 (2012).
[13]M. A. Binnewijzend, M. M. Schoonheim, E. Sanz-Arigita, A. M. Wink *et al.*, Neurobiol. Aging **33**, 2018 (2012).
[14]K. Supekar, V. Menon, D. Rubin, M. Musen *et al.*, PLoS Comput. Biol. **4**, e1000100 (2008).
[15]R. L. Buckner, A. Z. Snyder, A. L. Sanders, M. E. Raichle *et al.*, J. Cogn. Neurosci **12**(Suppl 2), 24 (2000).
[16]S. A. Rombouts, J. S. Damoiseaux, R. Goekoop, F. Barkhof *et al.*, Hum. Brain Mapp. **30**, 256 (2009).
[17]D. P. Kennedy, E. Redcay, and E. Courchesne, Proc. Natl. Acad. Sci. U.S.A. **103**, 8275 (2006).
[18]S. J. Weng, J. L. Wiggins, S. J. Peltier, M. Carrasco *et al.*, Brain Res. **1313**, 202 (2010).

[19]S. A. Rombouts, F. Barkhof, R. Goekoop, C. J. Stam *et al.*, Hum. Brain Mapp. **26**, 231 (2005).
[20]S. Bonavita, A. Gallo, R. Sacco, M. D. Corte *et al.*, Mult. Scler. **17**, 411 (2011).
[21]M. D. Greicius, B. H. Flores, V. Menon, G. H. Glover *et al.*, Biol. Psychiatry **62**, 429 (2007).
[22]I. M. Veer, C. F. Beckmann, M. J. van Tol, L. Ferrarini *et al.*, Front. Syst. Neurosci. **4**, 41 (2010).
[23]M. L. Kringelbach, A. L. Green, and T. Z. Aziz, Front. Integr. Neurosci. **5**, 8 (2011).
[24]K. J. Friston and C. D. Frith, Clin. Neurosci. **3**, 89 (1995).
[25]M. E. Lynall, D. S. Bassett, R. Kerwin, P. J. McKenna *et al.*, J. Neurosci. **30**, 9477 (2010).
[26]M. Liang, Y. Zhou, T. Jiang, Z. Liu *et al.*, Neuroreport **17**, 209 (2006).
[27]P. Skudlarski, K. Jagannathan, K. Anderson, M. C. Stevens *et al.*, Biol. Psychiatry **68**, 61 (2010).
[28]Y. Liu, M. Liang, Y. Zhou, Y. He *et al.*, Brain **131**, 945 (2008).
[29]D. S. Bassett, B. G. Nelson, B. A. Mueller, J. Camchong *et al.*, Neuroimage **59**, 2196 (2012).
[30]S. Kumra and S. Charles Schulz, Schizophr. Bull. **34**, 15 (2008).
[31]M. Kyriakopoulos and S. Frangou, Int. Rev. Psychiatry **19**, 315 (2007).
[32]J. Cabral, M. L. Kringelbach, and G. Deco, Pharmacopsychiatry **45**(Suppl 1), S57 (2012).
[33]G. Deco, A. Ponce-Alvarez, D. Mantini, G. L. Romani *et al.*, J. Neurosci. **33**, 11239 (2013).
[34]American Psychiatric Association (Ed.), *Diagnostic and Statistical Manual of Mental Disorders: DSM-IV-TR* (American Psychiatric Pub., 2000).
[35]J. Kaufman, B. Birmaher, D. Brent, U. Rao *et al.*, J. Am. Acad. Child Adolesc. Psychiatry **36**, 980 (1997).
[36]S. R. Kay, A. Fiszbein, and L. A. Opler, Schizophr. Bull. **13**, 261 (1987).
[37]G. Douaud, C. Mackay, J. Andersson, S. James *et al.*, Brain **132**, 2437 (2009).
[38]A. James, M. Hough, S. James, L. Winmill *et al.*, Schizophr. Res. **128**, 91 (2011).
[39]See supplementary material at http://dx.doi.org/10.1063/1.4851117 for the list of brain areas selected.
[40]N. Tzourio-Mazoyer, B. Landeau, D. Papathanassiou, F. Crivello *et al.*, Neuroimage **15**, 273 (2002).
[41]M. Jenkinson, P. Bannister, M. Brady, and S. Smith, Neuroimage **17**, 825 (2002).
[42]D. Collins, P. Neelin, T. Peters, and A. C. Evans, J. Comput. Assist. Tomogr. **18**, 192 (1994).
[43]T. E. Behrens, M. W. Woolrich, M. Jenkinson, H. Johansen-Berg *et al.*, Magn. Reson. Med. **50**, 1077 (2003).
[44]T. E. Behrens, H. J. Berg, S. Jbabdi, M. F. Rushworth *et al.*, Neuroimage **34**, 144 (2007).
[45]N. Brunel and X. J. Wang, J. Comput. Neurosci. **11**, 63 (2001).
[46]P. Theodoni, T. I. Panagiotaropoulos, V. Kapoor, N. K. Logothetis *et al.*, Front. Hum. Neurosci. **5**, 145 (2011).
[47]K. J. Friston, L. Harrison, and W. Penny, Neuroimage **19**, 1273 (2003).
[48]Y. He, J. Wang, L. Wang, Z. J. Chen *et al.*, PLoS ONE **4**, e5226 (2009)
[49]J. Wang, L. Wang, Y. Zang, H. Yang *et al.*, Hum. Brain Mapp. **30**, 1511 (2009).
[50]F. J. Massey, J. Am. Stat. Assoc. **46**, 68 (1951).
[51]M. Rubinov and O. Sporns, Neuroimage **52**, 1059 (2010).
[52]O. Sporns and J. D. Zwi, Neuroinformatics **2**, 145 (2004).
[53]O. Sporns and C. J. Honey, Proc. Natl. Acad. Sci. U.S.A. **103**, 19219 (2006).
[54]D. S. Bassett and E. Bullmore, Neuroscientist **12**, 512 (2006).
[55]O. Sporns, D. R. Chialvo, M. Kaiser, and C. C. Hilgetag, Trends Cogn. Sci. **8**, 418 (2004).
[56]D. J. Watts and S. H. Strogatz, Nature **393**, 440 (1998).
[57]L. Wang, C. Zhu, Y. He, Y. Zang *et al.*, Hum. Brain Mapp. **30**, 638 (2009).
[58]M. Hollander and D. A. Wolfe, *Wiley Series in Probability and Statistics Texts* (Wiley, 1999), references Sec. XIV.
[59]E. Bullmore and O. Sporns, Nat. Rev. Neurosci. **10**, 186 (2009).
[60]J. T. Coyle, G. Tsai, and D. Goff, Ann. N.Y. Acad. Sci. **1003**, 318 (2003).
[61]K. J. Friston, Acta Psychiatr. Scand Suppl. **99**, 68 (1999).
[62]G. Winterer and D. R. Weinberger, Trends Neurosci. **27**, 683 (2004).
[63]G. Winterer, Pharmacopsychiatry **39**, S68 (2006).
[64]D. C. Goff and J. T. Coyle, Am. J. Psychiatry **158**, 1367 (2001).
[65]G. Winterer, Curr. Opin. Psychiatry **23**, 112 (2010).
[66]A. Mobascher, T. Warbrick, J. Brinkmeyer, F. Musso *et al.*, Eur. Neuropsychopharmacol. **21**, S515 (2011).
[67]J. Cabral, E. Hugues, M. L. Kringelbach, and G. Deco, Neuroimage **62**, 1342 (2012).
[68]E. Bleuler, Allg. Z. Psychiatr. Psychischgerichtliche Med. **65**, 436 (1908).
[69]O. Sporns, *Networks of the Brain* (MIT Press, 2010).